Desalination and Water Treatment
www.deswater.com

doi: 10.5004/dwt.2020.26245

204 (2020) 124–135
November

Fabrication and characterization of cerium oxide nanoparticles for the removal of naphthol green B dye

Ayman A. Ali*, Sahar R. EL-Sayed, Sayed A. Shama, Talaat Y. Mohamed,Alaa S. Amin

Chemistry Department, Faculty of Science, Benha University, Benha City, Egypt, Tel. +201024857536; email: ayman.abdelrazik@fsc.bu.edu.eg (A.A. Ali)

Received 21 October 2019; Accepted 9 June 2020

ABSTRACT

The current research aimed for the fabrication of the cerium oxide nanoparticles using precipitation method and the as-fabricated sample was annealed at 400°C for 2 h. The fabricated sample was investigated using thermogravimetric analysis-differential thermal analysis, Fourier transform infrared, X-ray diffraction (XRD), field emission scanning electron microscopy, and high-resolution transmission electron microscopy. The extracted data from XRD showed that the annealed cerium oxide is in the nano-sized. The determined crystallite size equals 4.75 nm. The adsorption factors of naphthol green B dye (NGB) over the calcined CeO_2 were studied using a batch method. The adsorption capacity of the NGB dye over the fabricated CeO_2 nanoparticles (CEP4 sample) reaches 41 mg/g. Additionally, Langmuir adsorption isotherm and the pseudo-first-order kinetic models have utilized for the explanation of the adsorption process. Besides, the determined thermodynamics factors of the separation process showed spontaneous, physisorption, and endothermic process.

Keywords: Precipitation method; Cerium oxide nanoparticle; Adsorption; Morphology; Naphthol green B dye

1. Introduction

Water pollution is a relative concept where there is impure water according to its physical and chemical properties. Pure water can be contaminated using various pollutants such as heavy metals, organic dyes, pathogenic microbial materials, Pesticides, etc. Contaminated water that acts as a threat to human and it can't use in the field of industry. For example, a certain kind of mineral-free water can utilize in the electricity field. On the opposite side, the contaminated water with minerals and heavy elements, can't use because it corrodes the boiler in this industrial activity [1]. Organic pigments are the main source of environmental contamination of the pure water from textile, paper industries [2]. Dyes considered higher stable and complex to biodegrade because they usually are a difficult synthetic and complicated structure [3]. Dyes separated from wastewater by employing various advanced techniques [4] like adsorption, catalytic photodegradation, oxidation, flotation, coagulation, cloud-point extraction, electrodialysis, etc. Adsorption technique is a highly efficient separation process which is considered to be superior to water treatment other technologies. Adsorption technique characterized by many advantage points such as low cost, simplicity of setup and design, ease of operation, and sensitivity to different poisonous substances [5]. Naphthol Green B dye is an example of the common types of anionic dying for the pigmentation of various materials like wood, silk, cotton, etc. Naphthol Green B dye can produce some dangerous outcome in humans such as an increase in heart rate, shock, cyanosis, etc. Thus, the extraction of naphthol green B dye is very significant from different sources of wastewater because of its toxicity to living beings on our planet [5].

In the last three decades, many advanced types of nanomaterials have been developed and fabricated in different

* Corresponding author.

shapes and sizes. The synthesized nanomaterials utilized in numerous applications [6–10]. Between these nanomaterials, cerium oxide is one example of simple oxide with the chemical formula (CeO_2) [11]. CeO_2 is an example of the common reactive rare earth element oxides with a cubic fluorite-structured. The crystallographic structure does not change with the raising of the temperature to be more than 2,700°C (its melting point) [12,13]. In the cerium oxide structure, each Ce position is enclosed between eight oxygen sites in FCC arrangement and each oxygen position has a tetrahedron cerium site [14,15]. Cerium oxide nanoparticles interested extensive attention according to its important and unique characteristics such as UV absorbing ability, high thermal stability facile electrical conductivity, and diffusivity, high hardness, specific chemical reactivity, ability to store, and transport oxygen as large oxygen storage capacity. Because of these properties, it has been utilized for different classes of high-level applications like glass polishing material, buffer layers with a silicon wafer, gates for the metal-oxide-semiconductor device, solar cells, free radical scavenger, removal soot from diesel engine exhaust, separation of some organic materials from wastewater, water splitting for the fabrication of hydrogen gas, catalytic photodegradation under sunlight irradiation to many organic compounds, protective of primary cells from the detrimental effects of radiation therapy, and gas sensor [14].

CeO_2 nano-adsorbent fabricated by utilizing different methods like co-precipitation [16–18], sol–gel process [19–21], hydrothermal synthesis [22,23], reverse micellar synthesis [24,25], sonochemical synthesis [26,27], electrochemical synthesis [28,29], combustion synthesis [30], laser ablation [31], template [32], precursor thermal decomposition, and other methods [33]. In this paper, CeO_2 nanoparticles were fabricated by using a precipitation method because it is very simple, easy to set up and low cost. The fabricated cerium oxide nanoparticles (CEP4 sample) were applied for the removal and separation of naphthol green B dye (NGB) from aqueous solution. Also, the kinetics, thermodynamic and adsorption isotherm of naphthol green B dye (NGB) were investigated.

2. Experimental

2.1. Materials and reagents

Cerium sulfate tetrahydrate ($Ce(SO_4)_2{\cdot}4H_2O$, 98.5%) and naphthol green B dye ($C_{30}H_{15}FeN_3Na_3O_{15}S_3$, 99%) were purchased from Sigma-Aldrich Chemical Company (Germany). Nitric acid (HNO_3, 69%) and ammonium hydroxide (NH_4OH, 33%) were purchased from El Nasr Pharmaceutical Chemical Company (Cairo, Egypt). All chemicals and reagents were of analytical grade and utilized as received without any purification. Freshly bi-distilled water was utilized through all experiments. The chemical structure of the naphthol green B dye is displayed in Fig. 1.

2.2. Preparation of cerium oxide nanoparticles via precipitation method

0.01 mol of cerium sulfate tetrahydrate was dissolved in 50 mL bi-distilled water. Cerium hydroxide was precipitated by ammonium hydroxide (NH_4OH) until pH = 9.

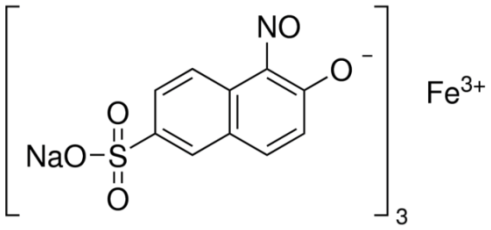

Fig. 1. Chemical structure of naphthol green B dye (NGB).

The obtained pale white precipitate was washed for several times and dried at 150°C for overnight (24 h), producing a pale-yellow powder (CEP sample). The obtained powder annealed at 400°C for 2 h and the crystalline CeO_2 nanoparticles (CEP4 sample) synthesized. The steps of the fabrication of CeO_2 nanoparticles are represented in a flowchart as shown in Fig. 2.

2.3. Characterization

The obtained phase of the as-fabricated (CEP sample) and annealed (CEP4 sample) cerium oxide was identified by measuring the X-ray diffraction (XRD) pattern analysis, 18 KW diffractometer (Bruker; model D 8 advance, USA) with monochromatic Cu-Ka radiation, 1.54178 (Å) in the angular range of 10°–80° with step size 0.02° (2θ) and scan step time 0.4 (s) and it was carried out at Central Metallurgical R&D Institute, Cairo, Egypt. The thermal analysis (thermogravimetric analysis (TGA), differential thermal analysis (DTA), and derivative thermogravimetry (DTG)) are used to test the as-fabricated products (CEP sample) and performed under air gas atmosphere using a thermal analyzer instrument (Shimadzu; model TA-60WS, Japan) with a heating rate of 10°C/min from 30°C to 800°C and it was

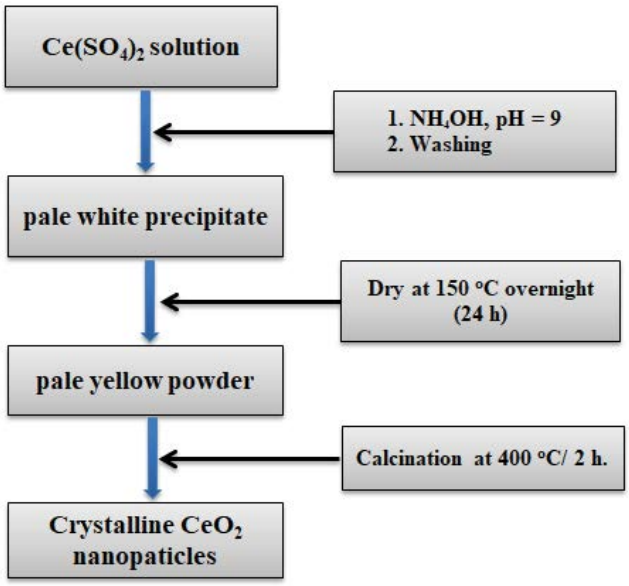

Fig. 2. Flow short of the preparation of cerium oxide using precipitation method.

performed at Egyptian Petroleum Research Institute, (Cairo, Egypt). The morphology of the calcined product (CEP4 sample) was studied using field emission scanning electron microscopy (FESEM, JEOL JSM-6390, USA). The (FE-SEM) and gold coating process by using EMITECH K550X sputter coater, England and it was performed at central laboratories, Egyptian Mineral Resources Authority, Cairo, Egypt. The morphology and particle size of the annealed cerium oxide (CEP4 sample) were confirmed using high-resolution transmission electron microscopy (HR-TEM) (model Tecnai G20, FEI, Netherland) at an electron voltage of 200 kV and it was carried out at Egyptian Petroleum Research Institute, Cairo, Egypt. The as-fabricated (CEP sample) and annealed (CEP4 sample) cerium oxide were measured using Fourier-transform infrared (FTIR) spectrometer (Thermo Scientific; model Nicolet iS10, Germany) from 4,000 to 400 cm^{-1}. It was performed at Chemistry Department, Faculty of Science, Mansoura University. The adsorption processes were tested using a Jasco UV-vis spectrophotometer (Jasco; model V 670, Japan) and it was carried at Chemistry Department, Faculty of Science, Benha University.

3. Result and discussion

3.1. Thermal analysis

TGA, DTA, and DTG curves of thermal analysis were recorded for as-fabricated cerium hydroxide (CEP sample) as to be visible in Fig. 3I. It also described the decomposition steps of the CEP sample which synthesized by the precipitation method. The decomposition of the CEP sample occurs in two steps as visible in the TGA curve. 16.25% was the total weight loss percentage from the CEP sample from 30°C to 500°C. In the first decomposition step, the adsorbed volatile molecules were separated and the removal from the CEP sample and the weight loss percentage found to be 8.5% in between 30°C and 200°C. The second decomposition step appeared in between 200°C and 500°C and the weight loss equals 7.75%. This step explains the decomposition of the CEP sample plus the evolution of the gases and the fabrication of cerium oxide nanoparticles. DTA curve exhibited an endothermic peak at 35°C and the volatile molecules separated from the surface of the CEP sample. Besides, the broad exothermic band observed in between 200°C and

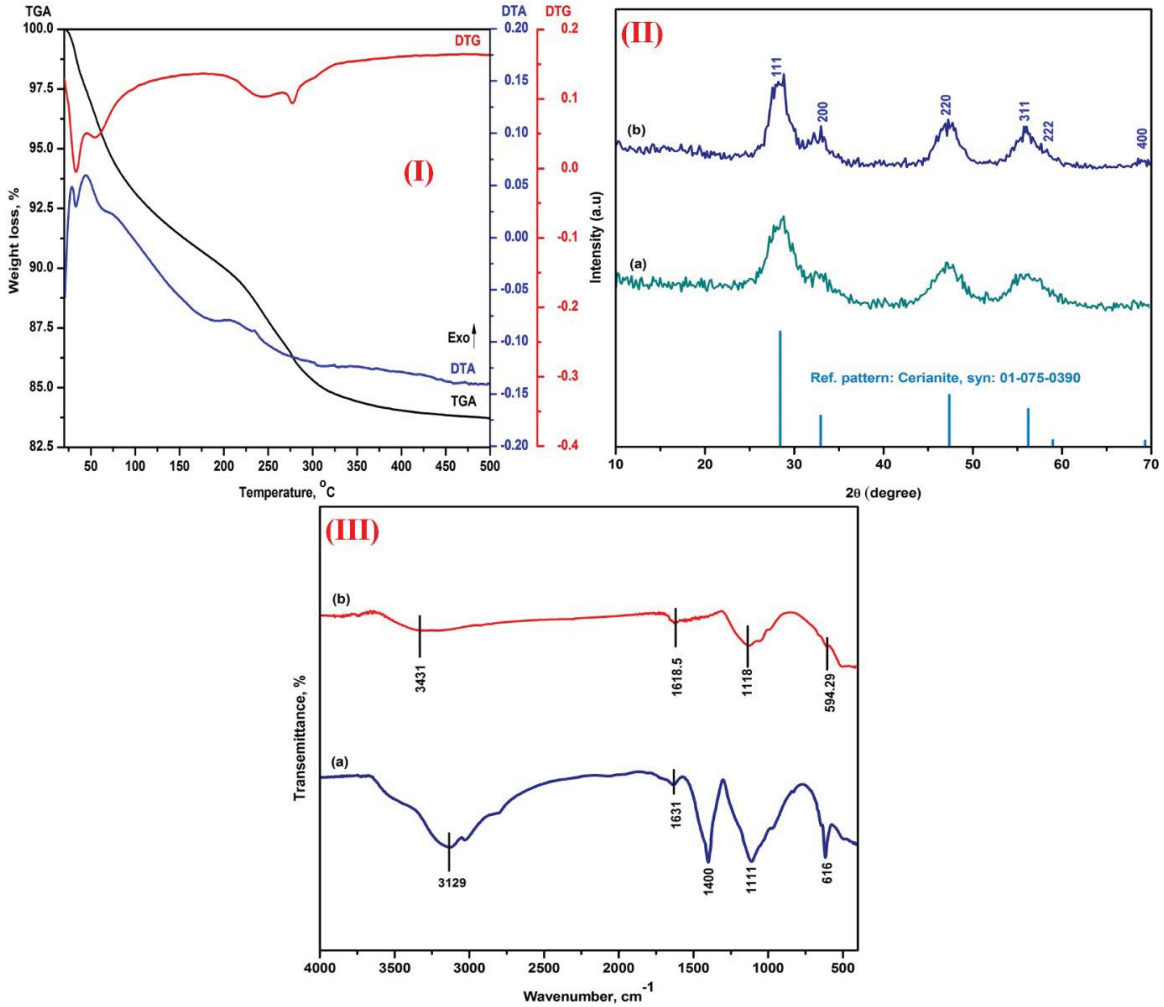

Fig. 3. Thermal analysis of CEP sample (I), XRD analysis (II), and FTIR analysis (III) of the synthesized cerium oxide (CEP (a) and CEP4 (b) samples).

245°C with two heads at 205°C and 235°C, is attributed to the evolution of the gases from the CEP sample. DTG exhibited the peaks at 35°C and 277°C and it agrees with the extracted data from the TGA curve. From the extracted data of the thermal analysis, CeO_2 nanoparticle (CEP4 sample) was obtained after the annealing at the selected temperature (400°C–500°C).

3.2. X-ray studies

Fig. 3II shows XRD patterns of the as-fabricated (CEP sample: curve a) and annealed cerium oxide nanoparticles at 400°C for 2 h (CEP4 sample: curve b). The appeared diffraction peaks are readily indexed to pure cubic phase structure of cerium oxide (CeO_2) which is in complete agreement with the standard patterns of CeO_2 (space group Fm-3m, Reference Card No.: 75–0390) for CeO_2 as exhibited in Fig. 3II. Other characteristic peaks corresponded to any impurities have not been seen. The crystal sizes of CeO_2 calculated by using the Debye–Scherrer formula [34] as shown in eq. (1). The average crystallite size (S) of the as-synthesized (CEP sample) and annealed (CEP4 sample) CeO_2 was recorded from the XRD peaks to be 4.13 and 4.75 nm, respectively.

$$S = \frac{0.9\lambda}{\beta\cos\theta} \tag{1}$$

where λ is the wavelength of X-ray (1.5406 A for Cu Kα), θ is the Bragg diffraction angle, and β is the X-ray full width of the diffraction peak at half-maximum height.

3.3. FT-IR spectrum

Infrared spectroscopy (FT-IR) of the as-fabricated (CEP sample: curve a) and annealed (CEP4 sample) CeO_2 samples (curve a) is displayed in Fig. 3III. Fig. 3III displays the FTIR spectra of the as-fabricated CEP sample without annealing (curve a). The peaks at 3,129 and 1,631 cm^{-1} are corresponding to the stretching and the bending vibrations of the adsorbed –OH groups, respectively. The peak at 1,400 cm^{-1} can be assigned to the symmetric vibration of adsorbed C=O. The peaks at 1,111 and 616 cm^{-1} in the spectra assigned to the vibration modes of Ce–O–Ce and Ce–O, respectively inside CeO_2 lattice. Fig. 3III displays the spectra of the annealed CEP4 sample (curve b). The weak absorption bands at 3,431 and 1,618.5 cm^{-1} are corresponding to the stretching and bending vibrations of hydroxyl groups respectively on the surface of CeO_2. The appeared peaks at 1,118 at 594 cm^{-1} in the spectra assigned to the vibration modes of Ce–O–Ce and Ce–O, respectively, inside CeO_2 lattice [13,33,35–39].

3.4. Morphology studies

The morphology of fabricated CeO_2 (CEP4 sample) was tested using HR-TEM and FE-SEM. The FE-SEM micrographs display that CeO_2 nanoparticles (CEP4 sample) are composed of the spherical nanoparticles in the form of the hard agglomeration as is visible in Figs. 4a–c. The average particle size determined from micrographs to be 50 nm. The HR-TEM micrographs reveal that the particles have different sizes of the round shape of CeO_2 nanoparticles (CEP4 sample) with hard agglomeration as shown in Figs. 4d–f. The average particle size of the CEP4 sample calculated to be 22 nm.

3.5. Batch adsorption experiments

The synthesized CeO_2 nanoparticles (CEP4 sample) utilized as an adsorbent for the separation of naphthol green B dye from aqueous solution using the batch mode. The amount of the dye adsorbed on the CEP4 sample and the removal efficiency percentage (R %) were calculated from Eqs. (2) and (3), respectively.

$$q_e = \frac{\left(C_0 - C_e\right)V}{m} \tag{2}$$

$$\text{Removal}\left(R\%\right) = \frac{\left(C_0 - C_e\right)}{C_0} \times 100 \tag{3}$$

where q_e is the amount of dye adsorbed per unit weight of adsorbent (mg/g), V is the volume of solution (L), C_0 is the initial dye concentration (mg/L), C_e is the equilibrium dye concentration (mg/L), and m is the weight of the adsorbent (g).

3.5.1. Effect of pH

Fig. 5i displays the effect of initial pH (3–9) on the adsorption of 50 mg/L of NBG dye solution over 50 mg of CEP4 sample. The removal efficiency recorded downward trend by increasing the pH values due to the electrostatic attractions between negatively charged functional groups located on the NGB dye and positively charged adsorbents surface as reported by other researchers [4,40,41]. The removal dye efficiency recorded at λ_{max} = 714 nm and it reached its maximum value (87.0%) at pH = 3.

3.5.2. Effect of contact time

The contact time of the removal 50 mg/L of NGB was tested using 50 mg of CEP4 sample at pH 3. Fig. 5ii shows the removal efficiencies for the NGB over CEP4 sample as a function of contact times ranging between 15 and 240 min. The rate of uptake was rapid in the beginning and became gradually in the latter stages until reached saturation state. The maximum separation and removal of NGB dye was attained in 150 min to be 21.9 mg/g.

3.5.3. Effect of initial concentration

Fig. 5iii displays the effect of various initial concentration for the separation of NGB dye over 0.05 g of CeO_2 (CEP4 sample), adjusting to pH = 3. After 150 min, the adsorption capacities were determined from the extracted data. The rate of uptake was rapid in the beginning and reached saturation as a result of the maximum availability of active sites on the surface of the CEP4 sample. As time passed, the active sites were blocked, the rate of the separation of dye decreased.

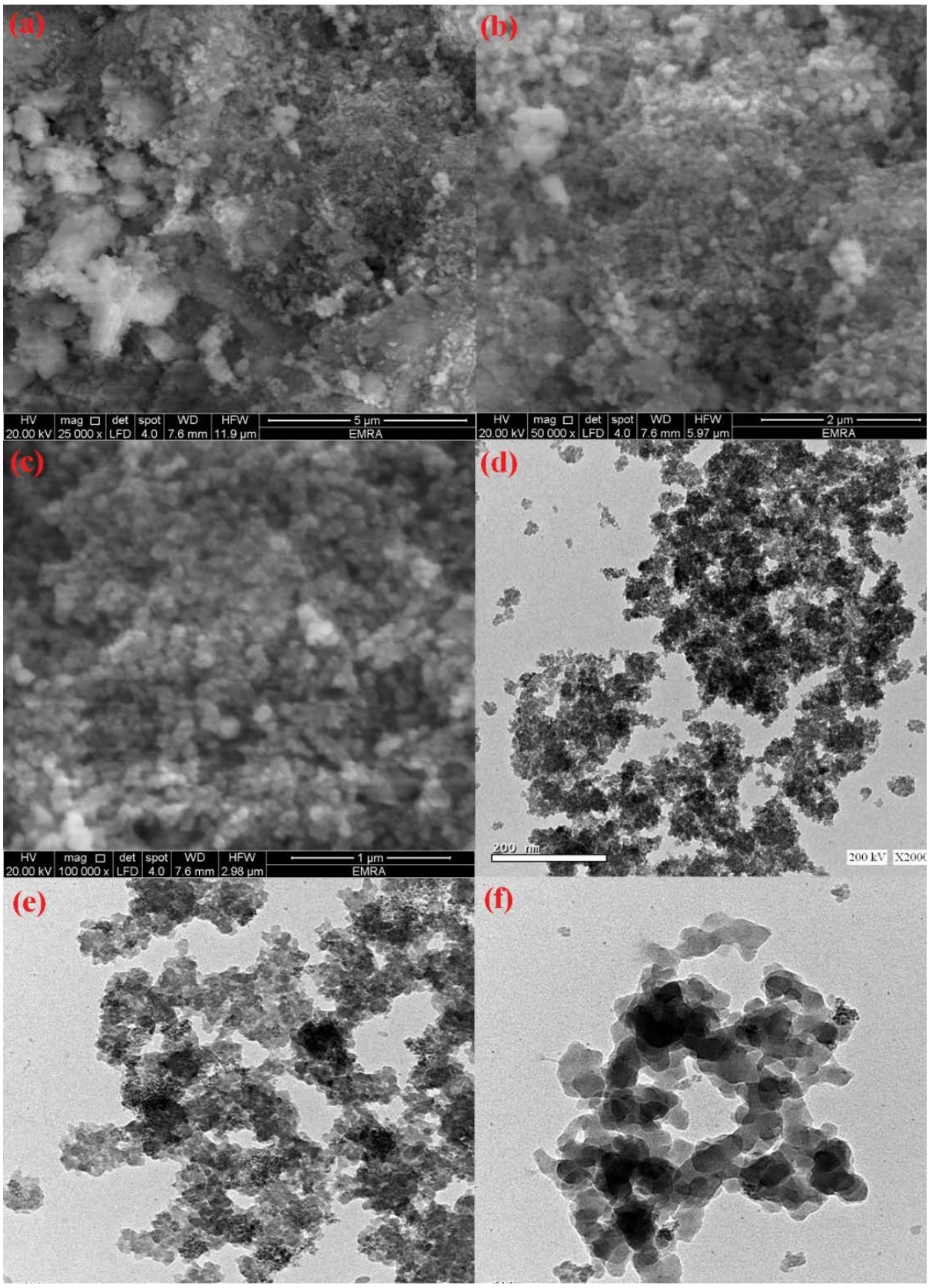

Fig. 4. FE-SEM images (a–c) and HR-TEM images (d–f) of the calcined cerium oxide nanoparticles (CEP4 sample).

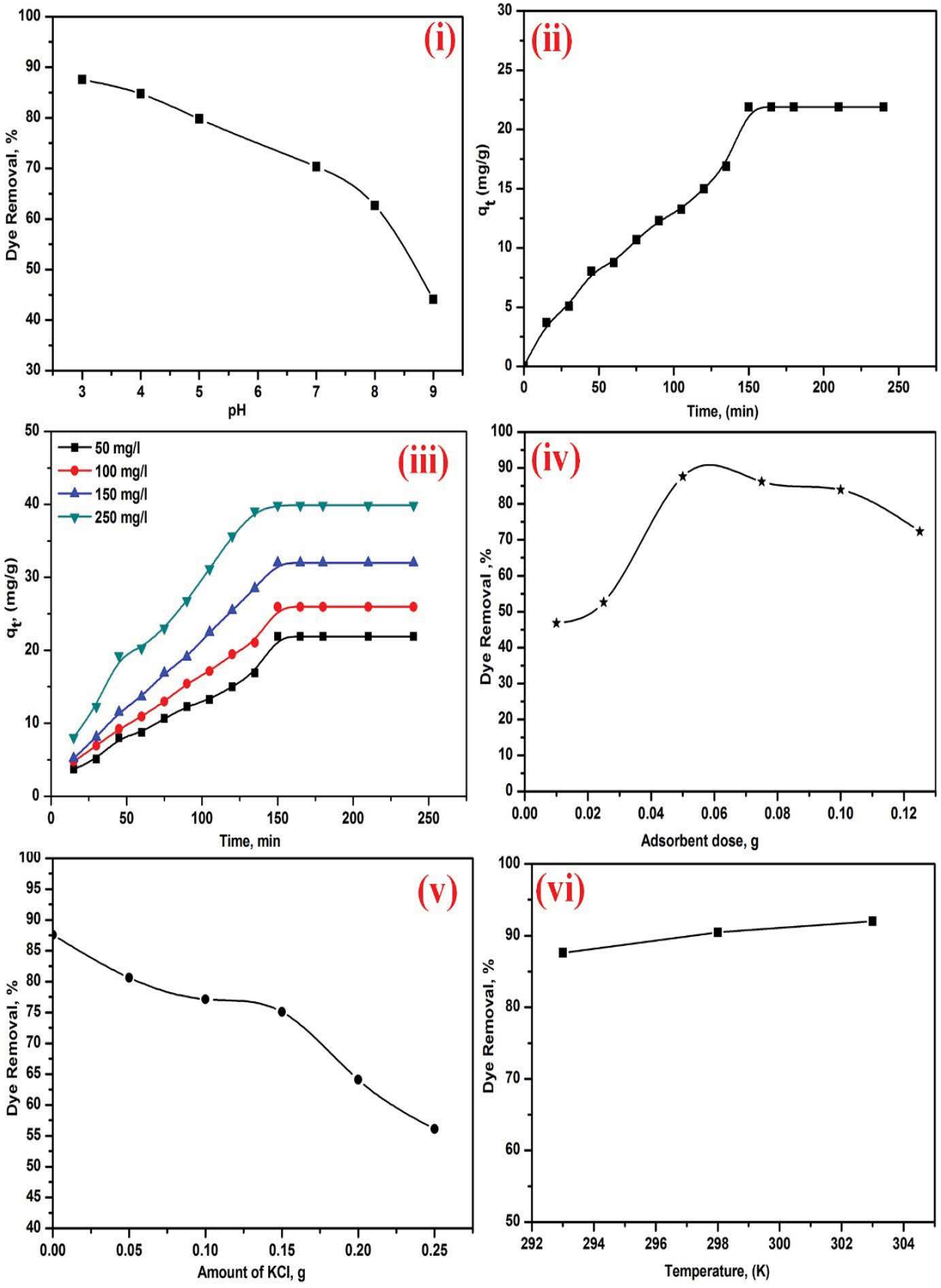

Fig. 5. Influence of pH (i), time (ii), initial concentration (iii), adsorbent dose (iv), ionic strength (v), and temperature (vi) on the removal of the NGB dye over the cerium oxide nanoparticle (CEP4 sample).

3.5.4. Effect of adsorbent dose

The effect of CeO_2 quantity on the removal 50 mg/L of NGB dye was investigated by adding various amount (0.01–0.125 g) of CEP4 sample as adsorbent and the pH of the solutions were fixed at 3. After 150 min, the efficiencies were calculated as shown in Fig. 5iv. The extracted data indicated that the increasing of adsorbent dosage leads to the increase of the separation of NGB dye on CEP4 material due to the rising of the active centre on the surface of CEP4 sample.

3.5.5. Effect of ionic strength

The effect of ionic strength on the adsorption 50 mg/L of NGB dye over 50 mg of CEP4 sample was investigated using different amount of KCl salt (0.05 to 0.25 g) at pH = 3. After 150 min, the removal efficiency calculated from the obtained data and the effect of ionic strength on the adsorption ability was demonstrated in Fig. 5v. As shown in Fig. 5v, the dose of KCl increases, the efficiency percentage of the separation of NGB dye decreases due to the decreasing active centre on the surface of CeO_2 (CEP4 sample) as result of the presence of KCl.

3.5.6. Effect of temperature

The adsorption process was tested at 293, 298, and 303 k separately for the separation 50 mg/L of NGB dye using 0.05 g of CeO_2 nano-adsorbent (CEP4 sample). The experimental data explain that the adsorption capacity increased slowly with an increase in the solution temperature for the separation of NGB dye over CEP4 sample as exhibited in Fig. 5vi. This indicates that the separation of NGB dye on the synthesized CeO_2 nano-adsorbent (CEP4 sample) is an endothermic process. The increase of temperature of the separation process was due to a decrease in the thickness of the boundary layer surrounding for the CEP4 sample and the mass transfer resistance of adsorbate in the boundary layer decreased. This leads to an increase in the mobility of the dye molecules with the rise of temperature.

3.6. Adsorption isotherms models of the separation of NGB dye over CeO_2 nanoparticles

The relation of the adsorption capacities with the various initial concentration of the dye (50–350 mg/L) as exhibited in Fig. 6a. The extracted data from relation shows the adsorption capacity increased until became constant after

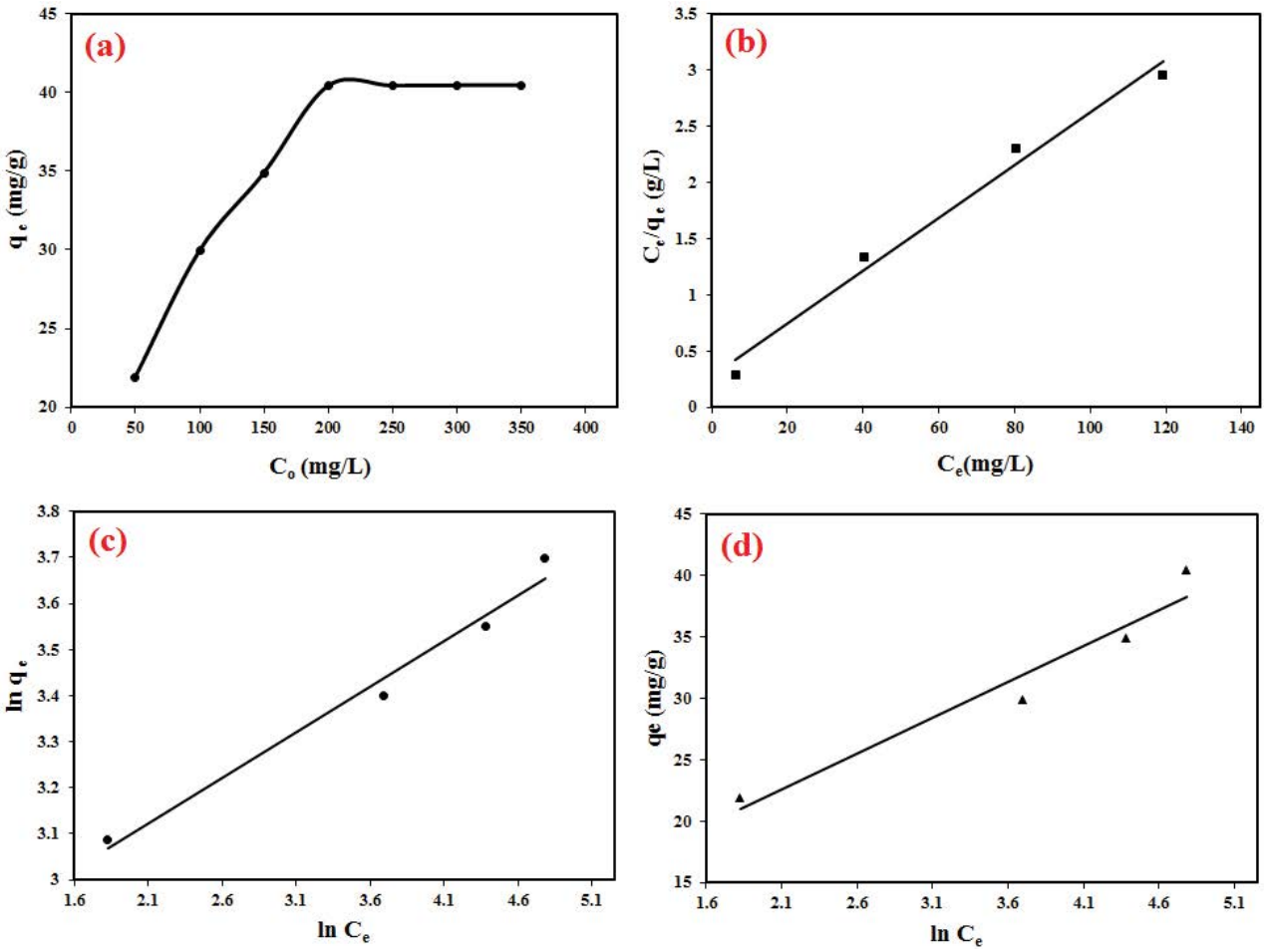

Fig. 6. Effect of initial concentration on the adsorption capacity (a), Langmuir (b), Freundlich (c), and Temkin (d) isotherms for removal the NGB dye using cerium oxide nanoparticles (CEP4 sample).

200 mg/L. The maximum value of the adsorption capacity was found at 41 mg/g. Temkin, Langmuir and Freundlich isotherm models are utilized for the description of the experimental data using different equilibrium concentrations of NGB dye (50–350 mg/L) over 0.05 g of CeO_2 nano-adsorbent (CEP4 sample) at pH = 3 and 293 K. After 150 min, the adsorption capacities determined and the adsorption factors estimated from the linear plots of Langmuir [4]. (C_e/q_e with C_e), Temkin [42,43] (q_e with $\ln C_e$) and Freundlich [44] ($\ln q_e$ with $\ln C_e$) isotherm models are displayed in Figs. 6b–d according to Eqs. (4)–(6), respectively.

$$\frac{C_e}{q_e} = \frac{1}{K_L q_m} + \frac{C_e}{q_m} \tag{4}$$

$$q_e = B \ln K_T + B \ln C_e \tag{5}$$

$$\ln q_e = \ln K_F + \frac{1}{Z} \ln C_e \tag{6}$$

where C_e is the equilibrium concentration of NGB dye in solution (mg/L), q_e is the equilibrium adsorption capacity of NGB dye on CeO_2 adsorbent (CEP4 sample), K_L is the Langmuir parameter (L/mg), q_m is the maximum quantity of adsorbed solute to adsorbent (mg/g). K_F is the Freundlich constant (mg/g), (1/Z) is the heterogeneity factor, B is constant ($B = RT/d$), K_T (L/g) is Temkin equilibrium binding constant corresponding to the maximum binding energy, and d is related to the heat of adsorption [45].

From Langmuir isotherm, the equilibrium parameter can calculate from $R_L = 1/(1+S)$, $S = K_L C_0$ and C_0 is the initial concentration of dye (mg/L) and the values of R_L reflects the nature of the adsorption process (if the values of R_L in between 0 and 1, the adsorption process is favorable). From Temkin isotherm can determine from $d = RT/B$, where T is the temperature in Kelvin and R is the universal gas constant (8.315 J/mol/K) [46]. From Freundlich isotherm, the maximum adsorption capacity can calculate using the relation: $q_m = K_f C_0^{1/z}$. If the value of $(1/Z) < 1$, it indicates normal adsorption. Besides, the value of Z in between $1 < Z < 10$, this indicates a favorable adsorption process [47]. Table 1 is outlined the factors were extracted from Langmuir, Temkin, and Freundlich isotherms. From the R^2 values, the Langmuir isotherm model is better fitting than the other models. It means that the uptake of the NGB dye over the CeO_2 nano-adsorbent (CEP4 sample) in the form of the homogenous surface by monolayer without any interaction between adsorbed molecules [48]. Besides, the estimated adsorption capacity from Langmuir isotherm was determined to be 42.55 mg/g which are closed with the experimental value (41 mg/g). In the current study, R_L values were determined in between 0.1880 and 0.05473 which is corresponding to the initial concentration 50–200 mg/g. It reflects that the adsorption of the NGB dye over the CEP4 sample is a favourable process. From the extracted data of Temkin isotherm, the heat of adsorption (d) has the value (0.4184 KJ/mol) and it reflects the weak interaction force between the surface of CeO_2 and NGB dye. Besides, the K_T found to be 5.963 L/g and the value of Temkin constant (B) found to be 5.823 J/mol. The R^2 value of Temkin equation found to be 0.9434 and it is lower than that obtained for the other isotherms.

Table 1
Extracted parameters from Langmuir, Freundlich, and Temkin isotherms for CeO_2 adsorbent (CEP4 sample)

Adsorption isotherm	Parameter	Values
Langmuir parameters	K_L (L/mg)	0.0864
	$q_{m,\text{cal}}$ (mg/g)	42.55
	R_L	0.05473–0.1880
	R^2	0.9828
	$q_{m,\text{exp}}$ (mg/g)	41
Freundlich parameters	K_F [(L/mg) (L/mg)$^{1/n}$]	14.9889
	$q_{m,\text{cal}}$ (mg/g)	42.77
	Z	5.0527
	R^2	0.9783
	$q_{m,\text{exp}}$ (mg/g)	41
Temkin parameters	K_T (L/g)	5.963
	d (KJ/mol)	0.4184
	B (J/mol)	5.8228
	R^2	0.9434

3.7. Adsorption kinetic models for the adsorption of NGB using CeO_2 nanoparticles

The adsorption kinetic models were carried out by studying the effect of contact time on the separation of NGB dye over CeO_2 adsorbent (CEP4 sample). Kinetic factors of the separation NGB dye on CeO_2 nano-adsorbent (CEP4 sample) were estimated using pseudo-first-order equation (plot $\log(q_e - q_t)$ against t) [49], pseudo-second-order equation (plot t/q_t vs. time t) [50], and intraparticle diffusion model (Plot q_t vs. $t^{0.5}$) [51] as represented in Eqs. (7)–(9). The relations were applied can get some information about the adsorbate quantity and the separation process rate through the calculation of kinetic factors as exhibited in Figs. 7a–c. The calculated data also outlined in Table 2.

$$\log\left(q_e - q_t\right) = \log q_e - \frac{k_1}{2.303} \tag{7}$$

$$\frac{t}{q_t} = \frac{1}{k_2 q_e^2} + \frac{t}{q_e} \tag{8}$$

$$q_t = k_1 t^{0.5} + D \tag{9}$$

where q_e and q_t are the amounts of dye adsorbed (mg/g) at equilibrium and time t (min), respectively, t (min) is contact time, and k_1 is the pseudo-first-order rate constant of adsorption (1/min), k_2 (g/mg min) is pseudo-second-order rate adsorption constant, k_I is intraparticle diffusion constant (mg/g min$^{0.5}$), and D is constant that gives an idea about the thickness of boundary layer (mg/g).

From Table 2 and depending on the R^2 values, the pseudo-first-order model is the better fitting (R^2 = 0.9854) than the pseudo-second-order (R^2 = 0.9715) for the

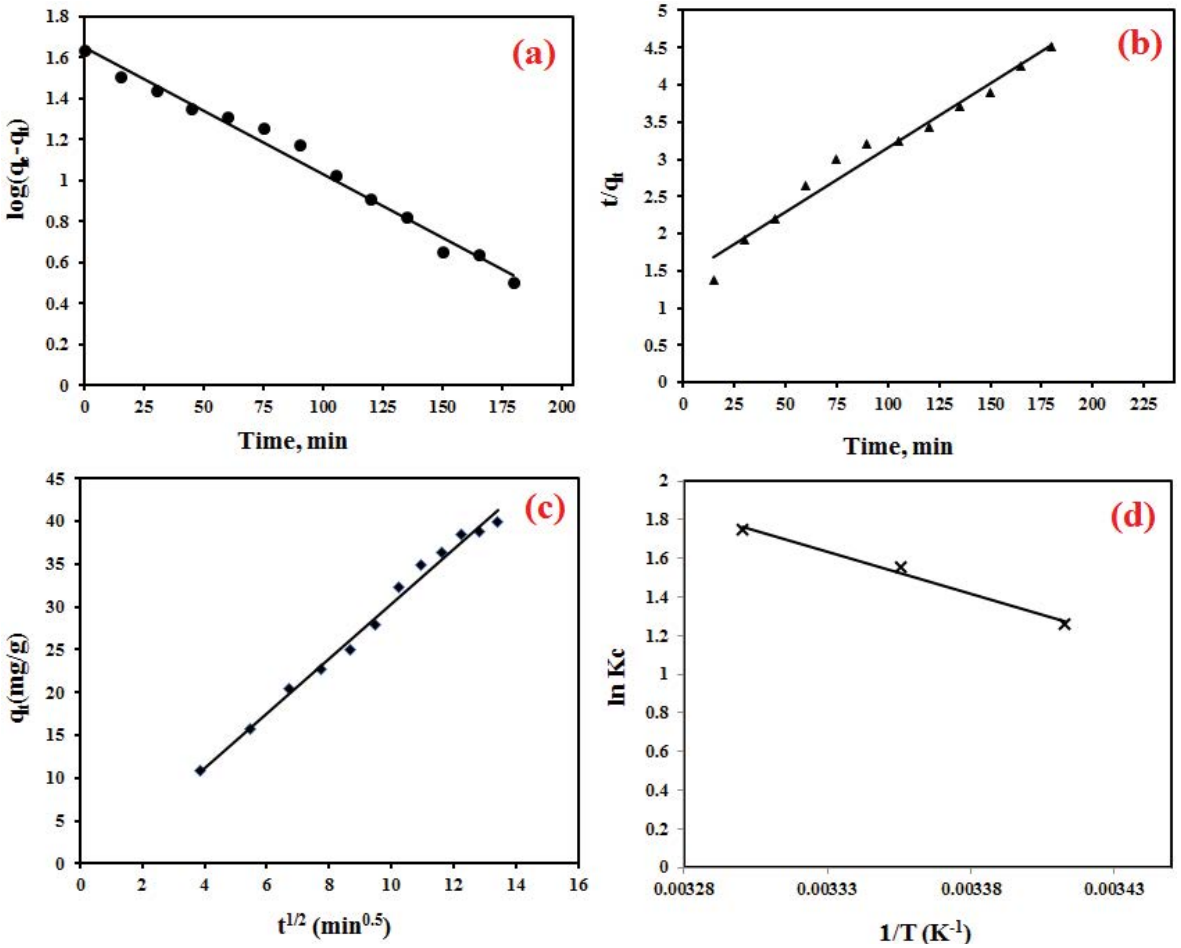

Fig. 7. Pseudo-first-order model (a), pseudo-second-order model (b), intra-particle diffusion model (c), and Van't Hoff relation (d) for removal the NGB dye over cerium oxide nanoparticles (CEP4 sample).

Table 2
Kinetic parameters for adsorption of NGB dye on CeO_2 adsorbent (CEP4 sample)

Kinetic parameters	Parameter	Values
Pseudo-first-order	k_1 (1/min)	0.014214
	$q_{m,cal}$ (mg/g)	44.77
	R^2	0.9854
Pseudo-second-order	$q_{m,exp}$ (mg/g)	41
	k_2 (g/mg.min)	0.00021
	$q_{m,cal}$ (mg/g)	57.79
	R^2	0.9715
Intra-particle diffusion	$q_{m,exp}$ (mg/g)	41
	k_I (mg/g $min^{0.5}$)	3.1923
	D (mg/g)	1.5026
	R^2	0.9901

separation of the NGB dye over CeO_2 nano-adsorbent (CEP4 sample). So, we can say that the separation of NGB dye over CeO_2 nanoparticles (CEP4 sample) follows the pseudo-first-order model and the calculated adsorption capacity value (cal. 44.77 mg/g) is in good agreement with the experimental one (41 mg/g). Fig. 7c displays the intra-particle diffusion model and the extracted values from linear relation: k_I = 3.1923 and D = 1.5026 mg/g. The plot does not pass the origin, and it is explained that the intraparticle diffusion is not the only model for the explanation mechanism of the separation process of dye over CeO_2 nano-adsorbent (CEP4 sample).

3.8. Thermodynamic studies for adsorbed of NGB dye using CeO_2 nanoparticles

The effect of temperature on the separation of NGB dye over CeO_2 nano-adsorbent (CEP4 sample) was tested in the temperature range: 293–303 K. The values of thermodynamic factors: $\Delta H°$, $\Delta S°$, and $\Delta G°$, were determined by using Van't Hoff equation [52], [Eq. (10)] as shown in Fig. 7d. The values of Gibbs free energy ($\Delta G°$) for separation NGB dye over CeO_2 nano-adsorbent (CEP4 sample) calculated from Eq. (11).

$$\ln K_C = \frac{\Delta S°}{R} - \frac{\Delta H°}{RT} \quad (10)$$

$$\Delta G^\circ = \Delta H^\circ - T\Delta S^\circ \quad (11)$$

where ΔH° is enthalpy change, ΔS° is entropy change, the values of K_c were determined from q_e/c_e and is the equilibrium constant (L/g), T is the temperature in Kevin (K), and R is the gas constant (8.314 J/mol). Plot $\ln(K_c)$ against $1/T$ gives a straight line as represented in Fig. 7d with slope $(-\Delta H^\circ/R)$ and intercept $(\Delta S^\circ/R)$.

All experimental constants are outlined in Table 3. The separation of NGB dye using CeO_2 nano-adsorbent (CEP4 sample) were endothermic process as a result of ΔH° has a positive charge. The value of ΔH° (cal. 36.11 KJ/mol) is lower than 40 KJ/mol, the separation and adsorption of NGB dye over CEP4 sample is the physisorption process [41,53]. ΔS° has a positive charge that means an increase in the degree of freedom of solution for the separation process. The negative values of ΔG° revealed that the separation process is spontaneous. Additionally, the ΔG° values decreased with increasing of temperature that means the separation of NGB dye is more favorable at high temperatures.

3.9. Comparative study

The adsorption capacities of CeO_2 nano-adsorbent (CEP4 sample) has been compared with other adsorbents reported in the literature and utilized for the removal of NGB dye. These collection data have been outlined in Table 4. The tabulated data show that CeO_2 nanoparticle (CEP4 sample) exhibits considerably higher adsorption capacity [4,41,54,55].

4. Conclusions

Cerium oxide nano-adsorbent was synthesized using the precipitation method and followed by the annealing at 400°C for 2 h. The fabricated samples were tested by employing different tools. The fabricated CeO_2 nano-adsorbent (CEP4 sample) has a small crystallite size after annealing (cal. 4.75 nm). From FTIR, the strong absorption band at 594 cm^{-1} are corresponding to the vibration modes of Ce–O band inside the lattice of CeO_2 nanoparticles. The optimum adsorption parameters of naphthol green B dye (NGB) over CeO_2 nano-adsorbent (CEP4 sample) were determined using a batch method. The maximum adsorption capacity of the NGB dye over CeO_2 nanoparticles (CEP4 sample) equals 41 mg/g. The separation data were well fitted with Langmuir adsorption isotherm and the pseudo-first-order. Besides, the adsorption and separation of naphthol green B dye on CeO_2 nano-adsorbent (CEP4 sample) was spontaneous, physisorption, and endothermic process.

Table 3
Thermodynamic parameters for the adsorption of NGB dye on the fabricated cerium oxide adsorbent (CEP4 sample)

Temperature, (K)	$\ln K_c$	ΔG° (KJ/mol)	ΔH° (KJ/mol)	ΔS° (KJ/mol)
293	1.2605	–3.108	36.11	0.1339
298	1.5552	–3.777		
303	1.7492	–4.446		

Table 4
Comparison of adsorption capacities (q_{max}) for various adsorbents

Adsorbents	Adsorption capacities, q_m (mg/g)	Reference
Tafla	23.86	[4]
Kaolinite	25.8	[4]
Charcoal	232.56	[4]
Metal hydroxides sludge (MHS)	10	[41]
SiO_2@Nap	79	[54]
Mg/Al-LDO	193.4	[55]
CEP4	41	This study

Acknowledgments

The authors express their thanks to Benha University, Egypt for support of the current research.

References

[1] M. AG, A. El Safty, M. Siha, Current situation of water pollution and its effect on aquatic life in Egypt, Egypt. J. Occup. Med., 37 (2013) 95–115.
[2] S. Gnanam, V. Rajendran, Facile sol-gel preparation of Cd-doped cerium oxide (CeO_2) nanoparticles and their photocatalytic activities, J. Alloys Compd., 735 (2018) 1854–1862.
[3] R. Riahi-Madvaar, M.A. Taher, H. Fazelirad, Synthesis and characterization of magnetic halloysite-iron oxide nanocomposite and its application for naphthol green B removal, Appl. Clay Sci., 137 (2017) 101–106.
[4] S. Rizk, M.M. Hamed, Batch sorption of iron complex dye, naphthol green B, from wastewater on charcoal, kaolinite, and tafla, Desal. Water Treat., 56 (2015) 1536–1546.
[5] W. Dai, H. Yu, N. Ma, X. Yan, Adsorption equilibrium and kinetic studies of crystal violet and naphthol green on torreya-grandis-skin-based activated carbon, Korean J. Chem. Eng., 32 (2015) 335–341.
[6] D. Malwal, G. Packirisamy, Chapter 10 – Recent Advances in the Synthesis of Metal Oxide (MO) Nanostructures, Synthesis of Inorganic Nanomaterials: Advances and Key Technologies (Micro and Nano Technologies), 1st ed., S. Mohan Bhagyaraj, O.S. Oluwafemi, N. Kalarikkal, S. Thomas, Eds., Woodhead Publishing-Elsevier Science, 2018, pp. 255–281, https://doi.org/10.1016/B978-0-08-101975-7.00010-5.
[7] A. Ali, M. Allazov, T. Ilyasli, Fabrication and study Tb^{3+}: $MgAl_2O_4$ by combustion method using malonic acid dihydrazide as fuel, Int. J. Adv. Sci. Technol. Res., 1 (2013) 358–367.
[8] A.A. Ali, I.S. Ahmed, Sol-gel auto-combustion fabrication and optical properties of cobalt orthosilicate: utilization as coloring agent in polymer and ceramic, Mater. Chem. Phys., 238 (2019) 121888–121902, doi: 10.1016/j.matchemphys.2019.121888.
[9] A.A. Ali, M.Y. Nassar, A.E.M. El Sharkwy, I.S. Ahmed, M. Abd, E.A. Elhalim, Fabrication and study of nickel oxide nanoparticles via low combustion synthesis method using different fuels, J. Basic Environ. Sci., 6 (2019) 183–186.
[10] A. Ali, B. Karasu, M. Allazov, T. Ilyasli, Synthesis, characterization and study of the effect of Yb^{3+} on $MgAl_2O_4$ spinel structure via combustion method, J. Chem., 3 (2013) 133–138.
[11] H. Balavi, S. Samadanian-Isfahani, M. Mehrabani-Zeinabad, M. Edrissi, Preparation and optimization of CeO_2 nanoparticles

and its application in photocatalytic degradation of reactive orange 16 dye, Powder Technol., 249 (2013) 549–555.
[12] G. Wang, Q. Mu, T. Chen, Y. Wang, Synthesis, characterization and photoluminescence of CeO_2 nanoparticles by a facile method at room temperature, J. Alloys Compd., 493 (2010) 202–207.
[13] S. Hassanzadeh-Tabrizi, M. Mazaheri, M. Aminzare, S. Sadrnezhaad, Reverse precipitation synthesis and characterization of CeO_2 nanopowder, J. Alloys Compd., 491 (2010) 499–502.
[14] S. Manikandan, A.A. Irudayaraj, A.D. Raj, M. Kirubanithy, Effect of precursor solution's pH on the properties of CeO_2 nanoparticles prepared by reflux method, Mater. Today: Proc., 2 (2015) 4378–4383.
[15] S. Supakanapitak, V. Boonamnuayvitaya, S. Jarudilokkul, Synthesis of nanocrystalline CeO_2 particles by different emulsion methods, Mater. Charact., 67 (2012) 83–92.
[16] M. Farahmandjou, M. Zarinkamar, T. Firoozabadi, Synthesis of cerium oxide (CeO_2) nanoparticles using simple co-precipitation method, Rev. Mex. Fis., 62 (2016) 496–499.
[17] C. Shih, Y. Chen, M. Hon, Synthesis and crystal kinetics of cerium oxide nanocrystallites prepared by co-precipitation process, Mater. Chem. Phys., 121 (2010) 99–102.
[18] J.-C. Chen, W.-C. Chen, Y.-C. Tien, C.-J. Shih, Effect of calcination temperature on the crystallite growth of cerium oxide nanopowders prepared by the co-precipitation process, J. Alloys Compd., 496 (2010) 364–369.
[19] T. Yu, J. Joo, Y.I. Park, T. Hyeon, Large-scale nonhydrolytic sol–gel synthesis of uniform-sized ceria nanocrystals with spherical, wire, and tadpole shapes, Angew. Chem. Int. Ed., 44 (2005) 7411–7414.
[20] N. Ferreira, R. Angélica, V. Marques, C. De Lima, M. Silva, Cassava-starch-assisted sol–gel synthesis of CeO_2 nanoparticles, Mater. Lett., 165 (2016) 139–142.
[21] A.A. Ansari, Optical and structural properties of sol–gel derived nanostructured CeO_2 film, J. Semicond., 31 (2010) 053001–053005, doi: 10.1088/1674-4926/31/5/053001.
[22] K. Kaneko, K. Inoke, B. Freitag, A.B. Hungria, P.A. Midgley, T.W. Hansen, J. Zhang, S. Ohara, T. Adschiri, Structural and morphological characterization of cerium oxide nanocrystals prepared by hydrothermal synthesis, Nano Lett., 7 (2007) 421–425.
[23] M. Hirano, E. Kato, Hydrothermal synthesis of cerium(IV) oxide, J. Am. Ceram. Soc., 79 (1996) 777–780.
[24] T. Masui, K. Fujiwara, K.-i. Machida, G.-y. Adachi, T. Sakata, H. Mori, Characterization of cerium(IV) oxide ultrafine particles prepared using reversed micelles, Chem. Mater., 9 (1997) 2197–2204.
[25] S. Sathyamurthy, K.J. Leonard, R.T. Dabestani, M.P. Paranthaman, Reverse micellar synthesis of cerium oxide nanoparticles, Nanotechnology, 16 (2005) 1960–1964.
[26] L. Yin, Y. Wang, G. Pang, Y. Koltypin, A. Gedanken, Sonochemical synthesis of cerium oxide nanoparticles-effect of additives and quantum size effect, J. Colloid Interface Sci., 246 (2002) 78–84.
[27] T. Alammar, H. Noei, Y. Wang, W. Grunert, A.-V. Mudring, Ionic liquid-assisted sonochemical preparation of CeO_2 nanoparticles for CO oxidation, ACS Sustainable Chem. Eng., 3 (2014) 42–54.
[28] Y. Zhou, R.J. Phillips, J.A. Switzer, Electrochemical synthesis and sintering of nanocrystalline cerium(IV) oxide powders, J. Am. Ceram. Soc., 78 (1995) 981–985.
[29] N.T. Nguyet, T. Trung, H. Lan, V. Van Thu, P.H. Vuong, P.D. Tam, Direct synthesis of CeO_2 nanospindles on gold electrode by electrochemical method, Vietnam J. Chem., 57 (2019) 57–63.
[30] T. Mokkelbost, I. Kaus, T. Grande, M.-A. Einarsrud, Combustion synthesis and characterization of nanocrystalline CeO_2-based powders, Chem. Mater., 16 (2004) 5489–5494.
[31] Y. Takeda, F. Mafuné, Formation of wide band gap cerium oxide nanoparticles by laser ablation in aqueous solution, Chem. Phys. Lett., 599 (2014) 110–115.
[32] C. Pan, D. Zhang, L. Shi, J. Fang, Template-free synthesis, controlled conversion, and CO oxidation properties of CeO_2 nanorods, nanotubes, nanowires, and nanocubes, Eur. J. Inorg. Chem., 2008 (2008) 2429–2436.
[33] C. Qizheng, D. Xiangting, W. Jinxian, L. Mei, Direct fabrication of cerium oxide hollow nanofibers by electrospinning, J. Rare Earths, 26 (2008) 664–669.
[34] P. Scherrer, Göttinger Nachrichten, Math. Phys., 2 (1918) 98–100.
[35] K.R. Alhooshani, Adsorption of chlorinated organic compounds from water with cerium oxide-activated carbon composite, Arabian J. Chem., 12 (2019) 2585–2596.
[36] S. Thakur, P. Patil, Rapid synthesis of cerium oxide nanoparticles with superior humidity-sensing performance, Sens. Actuators, B, 194 (2014) 260–268.
[37] T.N. Ravishankar, T. Ramakrishnappa, G. Nagaraju, H. Rajanaika, Synthesis and characterization of CeO_2 nanoparticles via solution combustion method for photocatalytic and antibacterial activity studies, ChemistryOpen, 4 (2015) 146–154.
[38] K. Babitha, A. Sreedevi, K. Priyanka, B. Sabu, T. Varghese, Structural characterization and optical studies of CeO_2 nanoparticles synthesized by chemical precipitation, Indian J. Pure Appl. Phys., 53 (2015) 596–603.
[39] L. Qian, J. Zhu, W. Du, X. Qian, Solvothermal synthesis, electrochemical and photocatalytic properties of monodispersed CeO_2 nanocubes, Mater. Chem. Phys., 115 (2009) 835–840.
[40] S. Yusra, H.N. Bhatti, Factors affecting biosorption of direct dyes from aqueous solution, Asian J. Chem., 22 (2010) 6625–6639.
[41] M. Attallah, I. Ahmed, M.M. Hamed, Treatment of industrial wastewater containing Congo red and naphthol green B using low-cost adsorbent, Environ. Sci. Pollut. Res., 20 (2013) 1106–1116.
[42] A. Dada, A. Olalekan, A. Olatunya, O. Dada, Langmuir, Freundlich, Temkin and Dubinin–Radushkevich isotherms studies of equilibrium sorption of Zn^{2+} unto phosphoric acid modified rice husk, IOSR J. Appl. Chem., 3 (2012) 38–45.
[43] B. Hameed, J. Salman, A. Ahmad, Adsorption isotherm and kinetic modeling of 2,4-D pesticide on activated carbon derived from date stones, J. Hazard. Mater., 163 (2009) 121–126.
[44] A. Agrawal, K. Sahu, B. Pandey, Removal of zinc from aqueous solutions using sea nodule residue, Colloids Surf., A, 237 (2004) 133–140.
[45] X.-s. Wang, Y. Qin, Equilibrium sorption isotherms for of Cu^{2+} on rice bran, Process Biochem., 40 (2005) 677–680.
[46] E.W. Shin, K. Karthikeyan, M.A. Tshabalala, Adsorption mechanism of cadmium on juniper bark and wood, Bioresour. Technol., 98 (2007) 588–594.
[47] S.V. Mohan, J. Karthikeyan, Removal of lignin and tannin colour from aqueous solution by adsorption onto activated charcoal, Environ. Pollut., 97 (1997) 183–187.
[48] Y. Bulut, Z. Tez, Adsorption studies on ground shells of hazelnut and almond, J. Hazard. Mater., 149 (2007) 35–41.
[49] L. Xiong, C. Chen, Q. Chen, J. Ni, Adsorption of Pb(II) and Cd(II) from aqueous solutions using titanate nanotubes prepared via hydrothermal method, J. Hazard. Mater., 189 (2011) 741–748.
[50] G. Akkaya, A. Özer, Biosorption of acid red 274 (AR 274) on dicranella varia: determination of equilibrium and kinetic model parameters, Process Biochem., 40 (2005) 3559–3568.
[51] F.-C. Wu, R.-L. Tseng, R.-S. Juang, Initial behavior of intraparticle diffusion model used in the description of adsorption kinetics, Chem. Eng. J., 153 (2009) 1–8.
[52] J.V. Milojković, M.L. Mihajlović, M.D. Stojanović, Z.R. Lopičić, M.S. Petrović, T.D. Šoštarić, M.Đ. Ristić, Pb(II) removal from aqueous solution by *Myriophyllum spicatum* and its compost: equilibrium, kinetic and thermodynamic study, J. Chem. Technol. Biotechnol., 89 (2014) 662–670.
[53] E.A. Abdelrahman, R.M. Hegazey, R.E. El-Azabawy, Efficient removal of methylene blue dye from aqueous media using Fe/Si, Cr/Si, Ni/Si, and Zn/Si amorphous novel adsorbents, J. Mater. Res. Technol., 8 (2019) 5301–5313.

[54] S. Chatterjee, H. Gohil, A.R. Paital, Dual functions of selective ferric ion detection and removal by a recyclable fluorescence active multifunctional silica material and toxic dye removal from aqueous solution, ChemistrySelect, 2 (2017) 5348–5359.

[55] F. Zhang, Z. Ni, S. Xia, X. Liu, Q. Wang, Removal of naphthol green B from aqueous solution by calcined layered double hydroxides: adsorption property and mechanism studies, Chin. J. Chem., 27 (2009) 1767–1772.